
Article:
Siddgonde, N., Quinn, J.A., O Brádaigh, C.M. et al. (2026) Mode I fracture toughness and compressive properties of glass fibre reinforced acrylic matrix composites before and after seawater ageing. Polymer Composites. ISSN: 0272-8397

https://doi.org/10.1002/pc.71033

Polymer Composites

WILEY | spe INSPIRING PLASTICS PROFESSIONALS

RESEARCH ARTICLE OPEN ACCESS

Mode I Fracture Toughness and Compressive Properties of Glass Fibre Reinforced Acrylic Matrix Composites Before and After Seawater Ageing

Nagappa Siddgonde[1,2] | James A. Quinn[1] | Conchúr M. Ó Brádaigh[3] | Dipa Ray[1]

[1]School of Engineering, Institute for Materials and Processes, The University of Edinburgh, Edinburgh, Scotland | [2]Department of Aerospace Engineering, Indian Institute of Technology Madras, Chennai, India | [3]Faculty of Engineering, University of Sheffield, Sheffield, UK

Correspondence: Nagappa Siddgonde (nagappa@iitm.ac.in) | Dipa Ray (dipa.roy@ed.ac.uk)

Received: 4 December 2025 | **Revised:** 2 March 2026 | **Accepted:** 5 March 2026

Keywords: compressive properties | glass fibre reinforced acrylic matrix composites | mode I interlaminar fracture toughness | seawater ageing | thermoplastic composites

ABSTRACT

Acrylic thermoplastic composites are emerging as a promising alternative for tidal and offshore wind turbine blades and marine applications, offering comparable structural performance and manufacturing process with improved end-of-life recyclability compared to traditional epoxy-based thermoset composites. The effect of seawater ageing (SWA) on various mechanical properties of glass fibre/acrylic matrix composites has been reported by some researchers; however, changes in Mode I fracture toughness and compressive performance of these composites under SWA conditions have not been reported. This paper reports the effect of SWA on the Mode I fracture toughness and compressive properties of glass fibre-reinforced acrylic matrix composites. Digital image correlation (DIC) was used to measure the surface strain field and monitor crack propagation during Mode I fracture toughness testing. The fracture toughness and compressive properties of the composites, in both dry and SWA conditions, revealed interesting observations that differ from more conventionally used thermoset matrices such as epoxy. The results indicated that SWA reduces the interlaminar fracture toughness, causing decreases of 25% in crack initiation and 14% in crack propagation energy compared to the dry samples. The glass transition temperatures were determined before and after SWA. The compressive modulus and strength were also measured before and after SWA, and the degradation mechanisms discussed, highlighting the impact of water ingress and plasticisation of acrylic matrix on mechanical performance. The fractographic analysis of the failed samples revealed further insights into the effects of water ingress and plasticisation on crack propagation behaviour.

1 | Introduction

Recently, acrylic resin-based thermoplastic composites are gaining attention in marine and renewable energy applications due to their recyclability [1]. Liquid acrylic resins have low viscosities (100–200 mPa s) at room temperature, and hence, these materials are well suited to processing by liquid composite moulding techniques using room-temperature tooling, which were once exclusively used for thermoset composite production. In addition, acrylic-based thermoplastic composites are also suitable for thick-section composites, which led to the design and development of thermoplastic composite blade components for renewable energy applications in recent years [1, 2].

During their lifespan, offshore wind turbine blades experience adverse environmental conditions such as temperature (–20°C to 50°C), high humidity (70%–100%), rain, snowfall and so forth. These factors significantly affect the mechanical, thermal and fracture toughness properties of the blade structures. Marine structures also undergo severe water ageing (SWA) during their

Highlights

- Investigated seawater ageing (SWA) effects on GF/acrylic composites.
- Mode I fracture and compressive properties after SWA revealed key insights.
- SWA reduced crack initiation and propagation by 14% and 25%, respectively.
- Fractography showed weaker fibre/matrix bonding in GF/acrylic composites after SWA.

service life, which alters their mechanical properties. This degradation occurs through processes such as water ingress, plasticisation, hydrolysis and interfacial debonding, ultimately weakening the composite and reducing its resistance to crack initiation and propagation within the composites [3–5]. Therefore, investigating the variation in mechanical properties under different environmental conditions is crucial for the broader acceptance of these materials in the renewable energy and marine sectors. Recently, some authors, including our group, have reported on the tensile, flexural, interlaminar shear strength and fatigue properties of both dry and SWA GF/acrylic composites [6–8]. The causes of reduction in the mechanical properties of acrylic composites are reported to be matrix plasticisation, swelling and degradation at the fibre–matrix interface [9–11]. The published papers report various levels of property drops in acrylic matrix composites due to SWA in comparison to a commonly used epoxy composite. This difference in property drops in different acrylic glass composite systems might be due to various grades of acrylic resins, glass fibres (GFs), sizing agents, various levels of interfacial bonding and void contents [11–13].

The degradation of the fibre/matrix interface in a composite due to ageing leads to a reduction in the fracture toughness of composite structures, because the fracture toughness mainly depends on the interfacial properties [3, 5, 12, 14]. This weakened interface can ultimately lead to catastrophic structural failures. Therefore, investigating fracture toughness of composites under such conditions is crucial. A few papers are available exploring the impact of environmental factors on Mode I fracture toughness of epoxy based thermoset composites, including the effects of temperature, humidity and salinity [4, 5]. Recently, several studies have examined the Mode I fracture toughness of acrylic composites in dry conditions. Bolluk et al. [15] studied the repair of GF/acrylic (Elium 188 O) composites using liquid resin injection and press moulding, focusing on Mode I fracture toughness and its recovery post-repair. Bhudolia et al. [16] studied the Mode I fracture toughness behaviour of carbon fibre (CF)/acrylic thick and thin ply systems considering an identical laminate thickness. Their study found that Mode I fracture toughness was 30% higher in thin ply CF/acrylic (Elium 280) composites than in thick ply CF/acrylic (Elium 280), and 72% higher than that in thin ply/epoxy composites. Recently, Kazemi et al. [17] investigated the compressive behaviour of various composites, including CF, Ultra-High-Molecular-Weight Polyethylene and fibre hybrids, fibre reinforcement of acrylic resin (Elium 188) composites under dry conditions. However, the fracture toughness and compressive performance of these composites under SWA conditions have not been reported. In particular, the Mode I fracture toughness and compressive properties of acrylic resin-based thermoplastic composites exposed to SWA remain largely unexplored. This study focuses on the effects of SWA on the Mode I fracture toughness and compressive properties of in situ polymerised GF/acrylic thermoplastic composites, manufactured using vacuum-assisted liquid resin infusion at room temperature. Dynamic mechanical analysis (DMA) and fractographic studies are also included to provide valuable insights into the structures of GF/acrylic composites after SWA.

The novelty of the present work lies in the systematic investigation of Mode-I interlaminar fracture toughness and compressive modulus and strength of GF/acrylic (Elium 191 SA/XO) thermoplastic composites under SWA conditions. To the best of the authors' knowledge, the combined evaluation of fracture and compressive performance of these acrylic-based thermoplastic composites after prolonged seawater exposure has not been previously reported in the open literature. This study provides new insights into the degradation mechanisms and mechanical performance evolution of GF/Acrylic thermoplastic composites in marine environments.

2 | Material and Experimental Methods

2.1 | Materials and Manufacturing

All laminates were prepared using a standard vacuum-assisted liquid resin infusion technique using unidirectional (UD) E-GF (UD-E-glass (16 μm)–1200 g/m^2, fabric width: 190 mm) with a 35 g/m^2 GF weft, stitched using 13 g/m^2 synthetic materials, procured from Saertex/Johns Manville, which contained an acrylic compatible sizing agent. Exact compositions of the acrylic compatible sizing agent are not known as this is proprietary with the GF manufacturer. The acrylic resins used were (Elium 191 XO/SA) and MEKP Butanox M50 was employed as the initiator. The mixing ratio of XO:SA resin was 50:50 by weight (%), and the initiator was added at a 100:3 ratio by weight (%). The [0°] four-layer laminates with a nominal thickness of 3.6 mm were fabricated for Mode I fracture toughness testing, incorporating a mid-plane pre-crack introduced by embedding a 13 μm-thick PTFE film during fabrication. Similarly, four-layer laminates with [0°] and [90°] orientations, each with a nominal thickness of 3.6 mm, were fabricated for compression testing.

2.2 | SWA

All Mode I Double Cantilever Beam (DCB) and compression samples designated for SWA were conditioned by immersion in natural seawater inside an environmental chamber maintained at 50°C. The seawater was collected from Portobello Beach, Edinburgh, Scotland. The SWA specimens were removed from the chamber and weighed at regular intervals of 24 h until they reached saturation. The objective was to investigate the change in properties after the samples were fully saturated with seawater. The percentage of mass increase was calculated using Equation (1), following ASTM D5229. In this equation, $M(t)$ represents the percentage increase in mass due to water uptake with respect to time t; W_o is the mass of the dry specimen and W_t is the mass of the specimen measured at time t.

$$M(t) = \frac{W_t - W_o}{W_o} \times 100 \quad (1)$$

A dry cloth was used to wipe the surface of all the samples to ensure that no water was present on the surface of the samples during weighing. All compression and DCB samples were immersed in a seawater bath for 150 days to undergo ageing (Figure 1c). All DCB samples were suspended in a seawater bath for ageing using a Perspex acrylic template, as shown in Figure 1c,d. This setup was primarily designed to prevent the degradation of the adhesive due to SWA, which was used to attach the loading blocks to the DCB samples. Additionally, images of both dry and SWA Mode I specimens are provided in Figure S1.

2.3 | Testing

2.3.1 | Fibre Volume Fraction (FVF)

The physical properties of the composites such as fibre, matrix and void volume fractions were measured using the matrix burn-off method following ASTM D3171 Method I. The densities of the GF/acrylic laminates, unreinforced acrylic polymer and GFs were measured using the displacement method in accordance with ASTM D792.

2.3.2 | Mode I Fracture Toughness Test

Mode I fracture toughness tests were performed on DCB specimens using an Instron 3369 fitted with a 10 kN loadcell following the ASTM D5528 standard. All Mode I DCB tests were performed under displacement-controlled mode at a constant crosshead speed of 3 mm/min in accordance with the ASTM D5528. The load–displacement response was recorded during the tests. DIC was used to monitor crack growth during the DCB tests. The dimensions of the DCB specimens are 175 mm × 25 mm × 3.6 mm (length × width × thickness).

2.3.3 | Compression Test

All compression tests were conducted in accordance with ASTM D6641 using an Instron 3369 testing machine equipped with a 50 kN load cell. The compression specimens measured 140 mm × 13 mm × 3.6 mm in length, width and thickness,

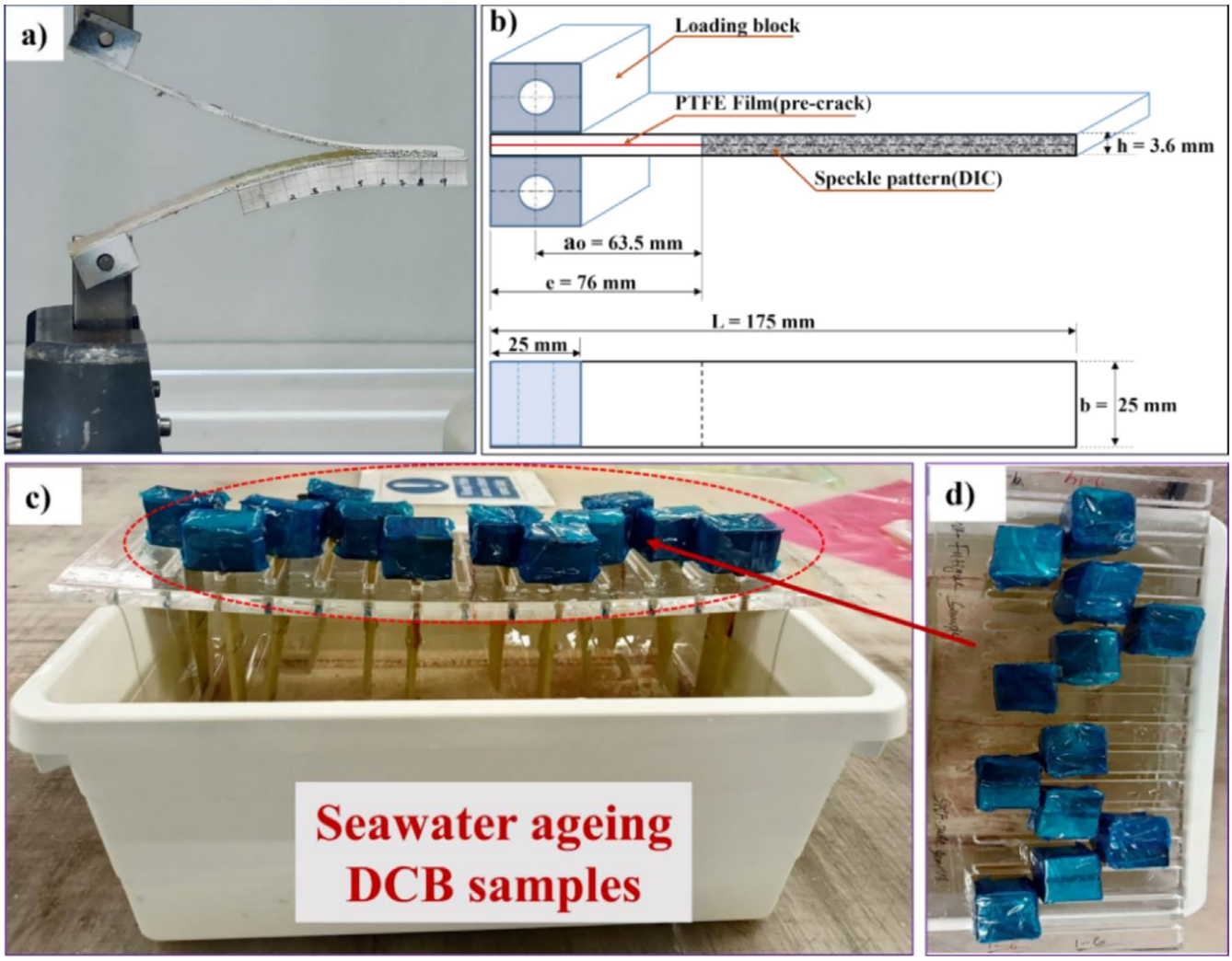

FIGURE 1 | Mode I fracture toughness (DCB) testing of GF/acrylic thermoplastic composite. (a) Test setup, (b) schematic diagram of DCB test specimen, (c) DCB samples immersed in seawater bath and (d) top view.

TABLE 1 | Physical properties of the GF/acrylic laminates.

Laminates	Laminate thickness (mm)	Lay-up sequence	Fibre volume fraction (%)	Void volume fraction (%)	Density ρ (kg/m^3)
DMA	1.95	$[0]_2$	53.31 ± 0.27	0.64 ± 0.32	1930 ± 20
Compression	3.57	$[0]_4$	55.92 ± 0.17	1.63 ± 0.2	1960 ± 8
Mode I	3.60	$[0]_4$	56.52 ± 0.09	1.38 ± 0.10	1970 ± 6

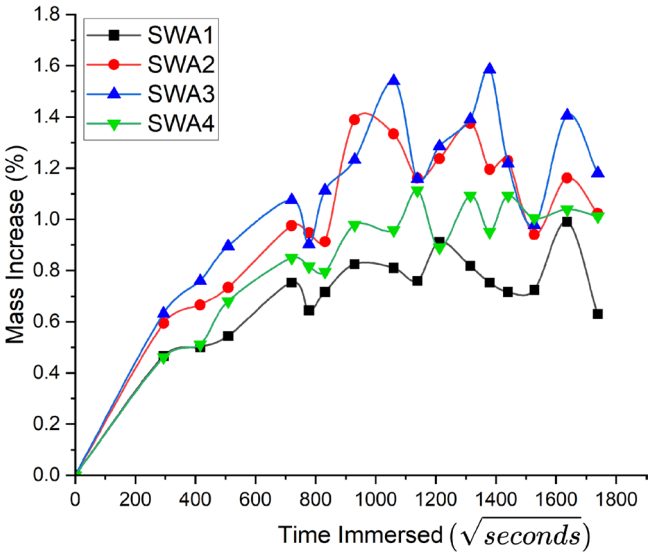

FIGURE 2 | The water absorption curves of GF/acrylic composite samples prepared for compression testing.

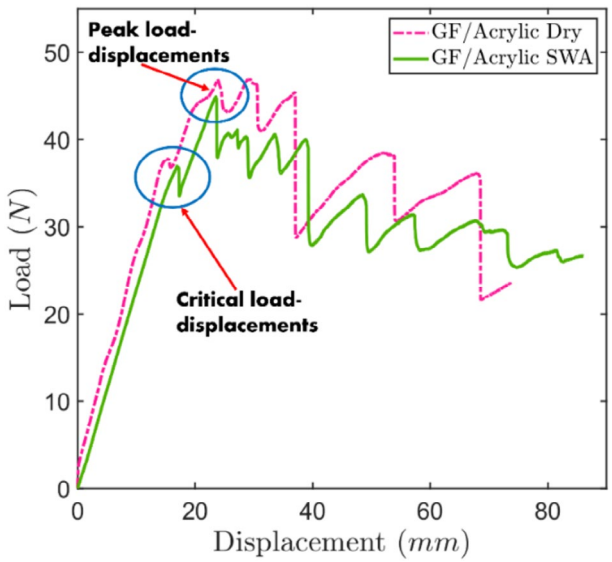

FIGURE 3 | Representative load–displacement response of DCB samples.

respectively. The compression specimens were speckled to facilitate measurement and recording of surface-apparent strains during testing using DIC. The specimens were tabbed with epoxy-glass composite untapered (square-ended) tabs to mitigate stress concentrations near the grips and to prevent buckling failure. Compression tests were performed on both [0°] and [90°] speckled specimens at a crosshead speed of 1.3 mm/min.

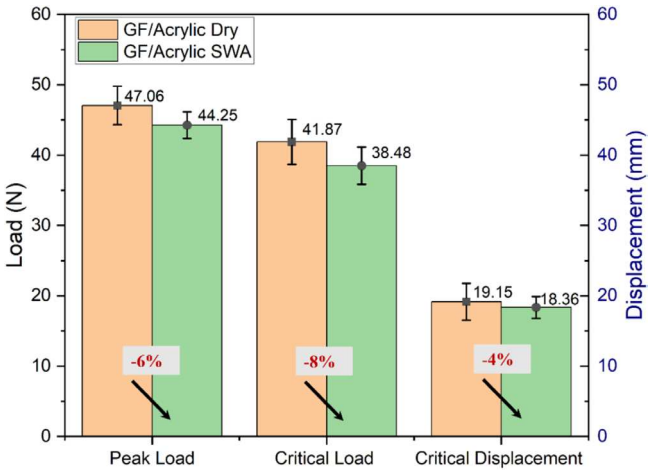

FIGURE 4 | Critical load–displacement and peak load values observed during Mode I fracture toughness test.

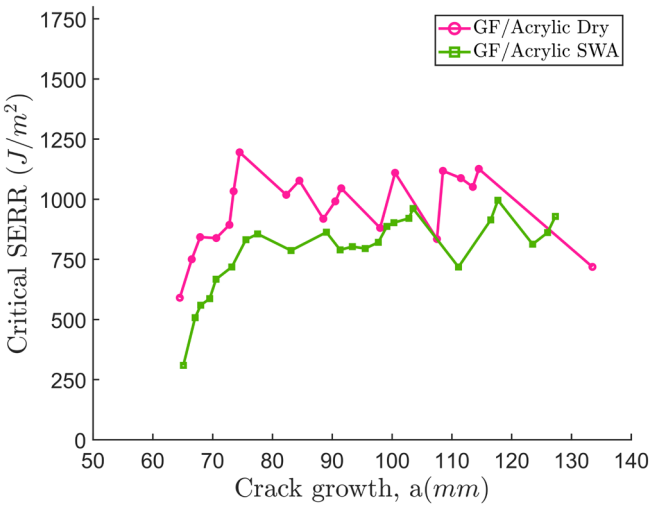

FIGURE 5 | Representative curve of critical SERR versus crack growth during Mode I fracture toughness tests, comparing dry and SWA conditions.

2.3.4 | DMA

DMA was performed with both dry and SWA samples to determine the glass transition temperature (T_g) using a TA Instrument DMA 850. Samples measuring 60×12×2 mm (length×width×thickness) with 0° orientation fibres along the span direction were tested in three-point bend at a frequency of 1.0 Hz and an amplitude of 20 μm. A ramp rate of 3°C/min between ambient temperature and 180°C was used and three specimens were tested for each dry and SWA set. SWA samples were

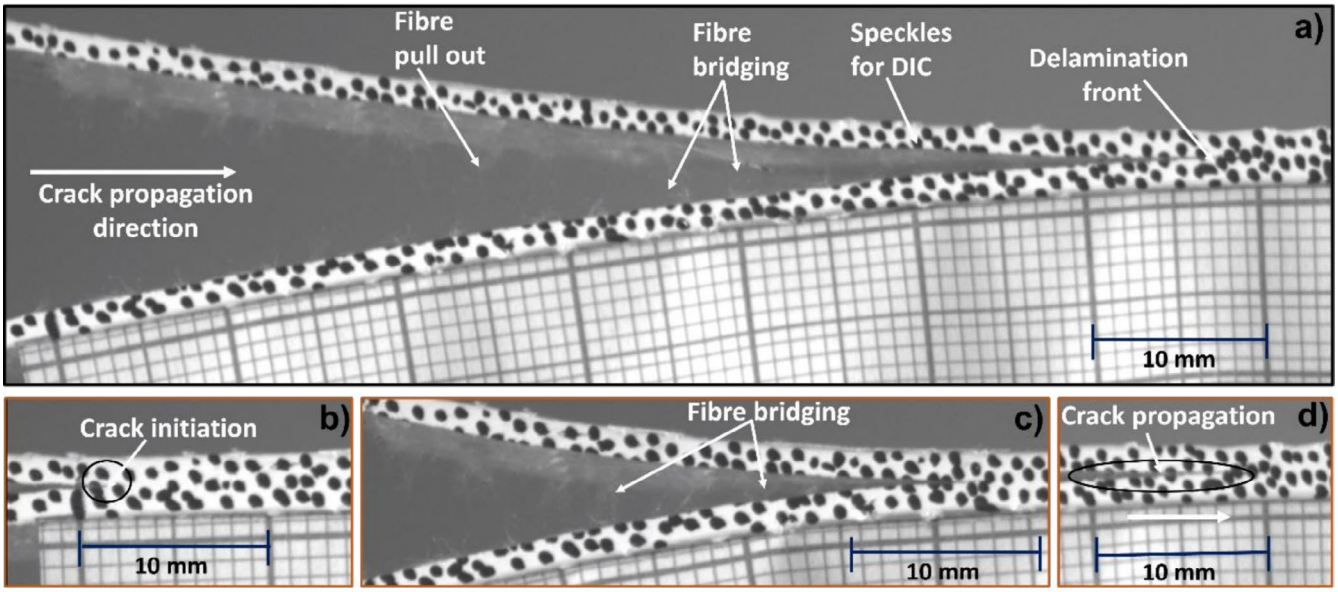

FIGURE 6 | (a) Macro-photographs of the side surface of the DCB specimen, along with a detailed depiction of the Mode I fracture mechanism in the GF/acrylic laminate including: (b) crack initiation, (c) fibre bridging and (d) crack propagation.

removed from the water bath, wiped with a dry cloth to remove the surface water and then tested immediately. Additionally, to study the recovery properties, one of the SWA samples was dried in the open-air for 24 h before testing.

2.3.5 | Scanning Electron Microscopy (SEM)

The fracture surfaces of the DCB tested samples were sputter-coated with a 30 nm layer of gold to enhance surface conductivity before imaging. SEM was then conducted on the fracture surfaces using a JEOL microscope operated at an acceleration voltage of 15.0 kV.

2.3.6 | Statistical Analysis

The Mode I fracture and compression test results were analysed using statistical methods to assess the significance of their variance. A statistical *t*-test was used to determine whether a significant difference exists between the means of two groups of values. The Equation (2) used to calculate the *t*-test values is as follows:

$$t = \frac{(x_1 - x_2)}{\sqrt{\frac{(s_1)^2}{n_1} + \frac{(s_2)^2}{n_2}}} \quad (2)$$

where t is the *t*-test value, x represents the sample mean, s denotes the standard deviation and n is the number of samples.

3 | Results and Discussion

In this section, all compression and DCB results are discussed based on a minimum of five samples per test type. Additionally, DMA and burn-off tests were conducted, with results reported for three and four samples, respectively. Also, all these experimental results under dry and SWA conditions are tabulated in Table S1.

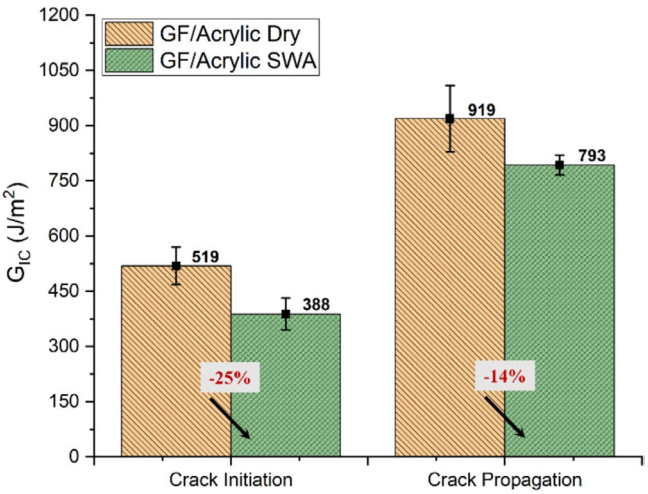

FIGURE 7 | Mode I fracture toughness, G_{IC}, values during crack initiation and propagation in GF/acrylic laminate specimens under dry and SWA conditions.

3.1 | FVF

The density of the GF/acrylic laminates was calculated according to Archimedes principle, as specified by ASTM D792. The average densities of the GF and polymerised acrylic resin were measured to be 2600 and 1184 kg/m^3, respectively. The FVFs and void contents were determined through burn-off tests. Four samples from each set were tested for all laminates used in mechanical tests. The corresponding FVF values are presented in Table 1.

3.2 | Water Absorption

The water uptake of four SWA compression samples is plotted as a function of the square root of immersion time, as shown in Figure 2. The average water uptake curves for these samples are provided in Figure S2. The observed percentage of mass increase

was minimal at 1%, which can be attributed to the low void content (1.6%) in the GF/acrylic laminate. A similar mass increase (0.8%) was reported in our previous works on GF/acrylic composites where the GF had a multi-compatible sizing (MCS) agent [6]. This increase is also similar to a previous work on GF/powder epoxy composite where a 1% increase in mass was reported on SWA [4]. All [0°] and [90°] samples were immersed in seawater for 150 days prior to testing.

3.3 | Mode I Fracture Toughness

The Mode I fracture toughness of GF/acrylic laminates was determined in both dry and SWA conditions. Figure 1a shows the DCB test setup, while Figure 1b illustrates the schematic of the DCB samples used in the study. The representative load-displacement curves from DCB tests for both dry and SWA samples are shown in Figure 3. The crack initiation was observed before the maximum peak load for both dry and aged samples, as shown in Figure 3. After the peak load, crack propagation eventually completed with the increase in displacement with respect to load drops in both dry and SWA samples. The critical load–displacement points and the peak load–displacement responses are highlighted in Figure 3. Compared to dry specimens, the SWA load–displacement curves showed that lower loads were required to initiate and propagate in the SWA samples, which can be attributed to water ingress, matrix plasticisation and weakening of the fibre/matrix interfacial bond. As a result, the critical load and displacement values in the SWA samples were reduced by 8%

TABLE 2 | Summary of Mode I fracture toughness studies on dry E-glass composites with different resin systems.

Composite system	Mode I G_{IC} (J/m^2)		References	Resin type	Fabric sizing
	Init.	Prop.			
GF/acrylic	520	919	This study	Elium 191 XO/SA	AS-JM
GF/acrylic	556	1814	Obande et al. [19]	Elium 188 O	MCS-AM
GF/acrylic	413	978	Bolluk et al. [15]	Elium 188 O	AS-JM
GF/acrylic	590	940	Han et al. [20]	Elium 150	UD-GF
GF/epoxy	446	1574	Obande et al. [19]	SR 1710	MCS-AM
GF/epoxy	346	768	Hassan et al. [3]	Z-epoxy 300	UD-GF
GF/epoxy[a]	1643	1939	C. Floreani [4]	EC-CEP-0016	UD-GF

Abbreviation: AS-JM: acrylic sizing from John Manville, MCS-AM: multi-compatible sizing from Ahlstrom-Munksjö.
[a]GF/powder-epoxy method, UD-GF: uni-directional stitched GF, no sizing agent mentioned.

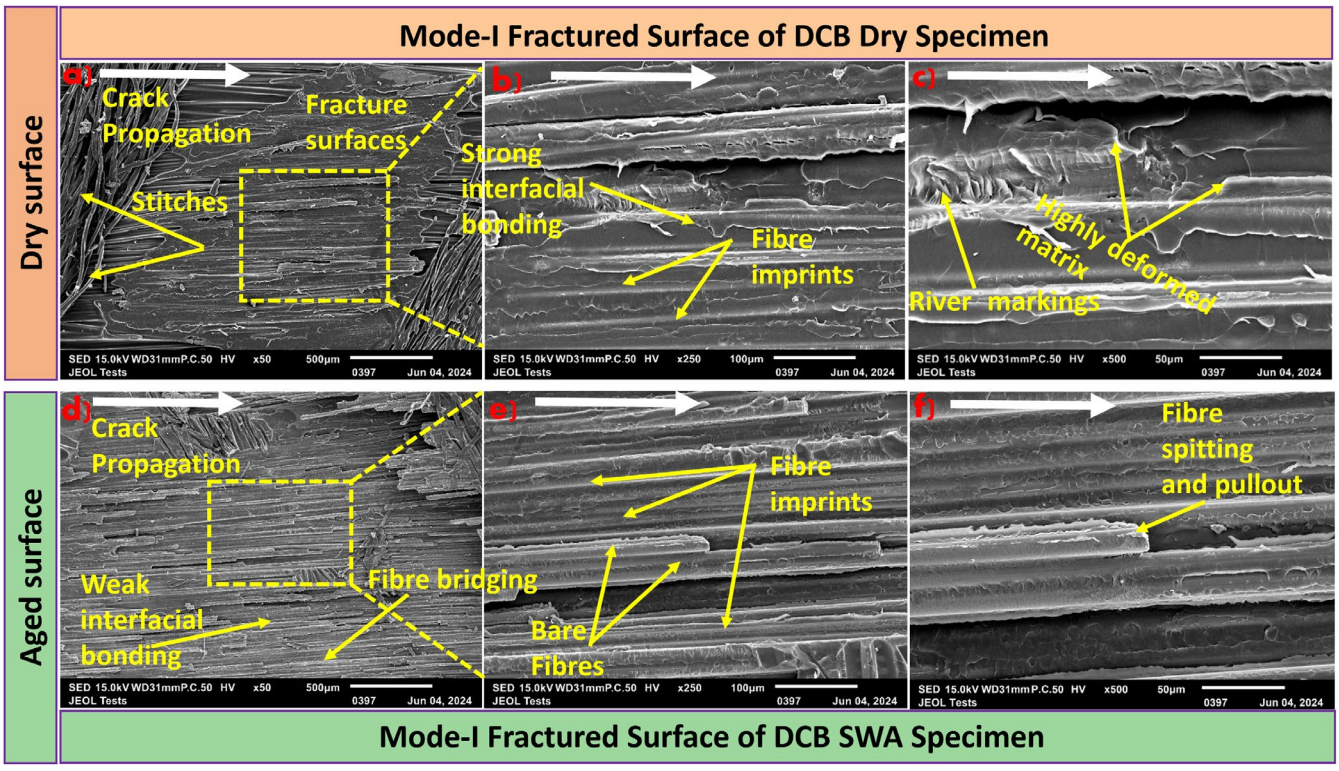

FIGURE 8 | SEM images of Mode I fracture surfaces of dry and SWA specimens of GF/acrylic laminates.

and 4%, respectively, with a 6% reduction in peak load compared to the dry samples, as shown in Figure 4.

However, the reduction in critical load and critical displacement values in SWA samples, compared to dry samples, was not proven to be statistically significant, as determined by a *t*-test analysis with $p = 0.091$ and $p = 0.0567$, respectively, at a significance level of $\alpha = 0.05$. In contrast, the reduction in peak load between dry and SWA samples was found to be statistically significant ($p = 0.041$, $\alpha = 0.05$). The critical strain energy release rate (SERR) G_{IC}, for both dry and SWA samples was calculated from the experimentally obtained load–displacement curves using modified beam theory (MBT), as shown in Equation (3).

$$G_{IC} = \frac{3P\delta}{2b(a + |\Delta|)} \times \frac{F}{N};\ a = \left(a_{o+}\, a_i\right) \tag{3}$$

where b is the width of the DCB specimen, δ is the displacement, P is the applied load and $|\Delta|$ is the correction factor for rotation at the crack tip of the DCB specimen. Similarly, a_o represents the initial crack length and a denotes the measured crack length, including the initial crack (a_o); F and N are correction factors determined from the experimental data by generating linear regression of the cubic root of compliance ($C^{1/3}$) against the delamination length (a). The critical SERR with respect to the crack growth curve is shown in Figure 5.

Fluctuations in the SERR curves were observed, and they can be caused by various factors such as fibre bridging during the crack propagation, the presence of stitching in the glass fabric and interaction between inter-laminar cracks [18], as shown in Figure 6. The fluctuations in the critical SERR curve of SWA samples are comparatively less pronounced than in dry samples,

FIGURE 9 | Compression test setup with [0°] and [90°] oriented composite specimens.

which can be attributed to the effect of matrix plasticisation. It is also observed that the drop in the SERR curve in the SWA samples was significant. Figure 7 highlights a substantial decrease in Mode I fracture toughness G_{IC} (J/m^2) for the SWA samples, with reductions of 25% and 14% for crack initiation and propagation, respectively. Further, all supporting data including load–displacement curves and critical ERR versus crack length plots for both dry and SWA samples along with their comparisons are provided in Figures S3–S6.

The reduction in both crack initiation and propagation values in SWA samples, compared to dry samples, was statistically significant, as determined by a *t*-test analysis with $p = 0.0017$, $p = 0.027$, respectively, at a significance level of $\alpha = 0.05$. This indicates a more pronounced energy drop during crack initiation than during propagation in the SWA samples. Similarly, our previous work on GF/powder-epoxy composites under SWA reported 30% and 25% drops in crack initiation and propagation, respectively [4], though the overall values were nearly twice as high for the powder-epoxy materials (Table 2).

A study by Hassan et al. [3] reported a 30% decrease in Mode I fracture toughness (propagation) for glass/epoxy composites after 24 days of water immersion and a 55% decrease after 35 days, compared to dry samples. In contrast, in our study, acrylic resin-based thermoplastic composites exhibited a relatively smaller reduction in both initiation (14%) and propagation (24%) fracture toughness values after ageing for 150 days. Literature results for CF/acrylic (Elium) and GF/acrylic (Elium) laminates in dry condition demonstrated better crack resistance in both initiation and propagation phases ($G_{ICi} = 556$ J/m^2, $G_{ICp} = 1814$ J/m^2), leading to higher fracture toughness values compared to conventional epoxy composites ($G_{ICi} = 446$ J/m^2, $G_{ICp} = 1574$ J/m^2) [19, 21]. This can be attributed to strong fibre-matrix bonding and global plastic deformation of the acrylic matrix (Figure 8a). This trend is also evident in previous studies as summarised in Table 2. The Mode I fracture toughness of GF/acrylic laminates for only dry condition with different grades of Elium resin, different types of GF with various sizing agents and GF/epoxy laminates are summarised in Table 2 for a comparison.

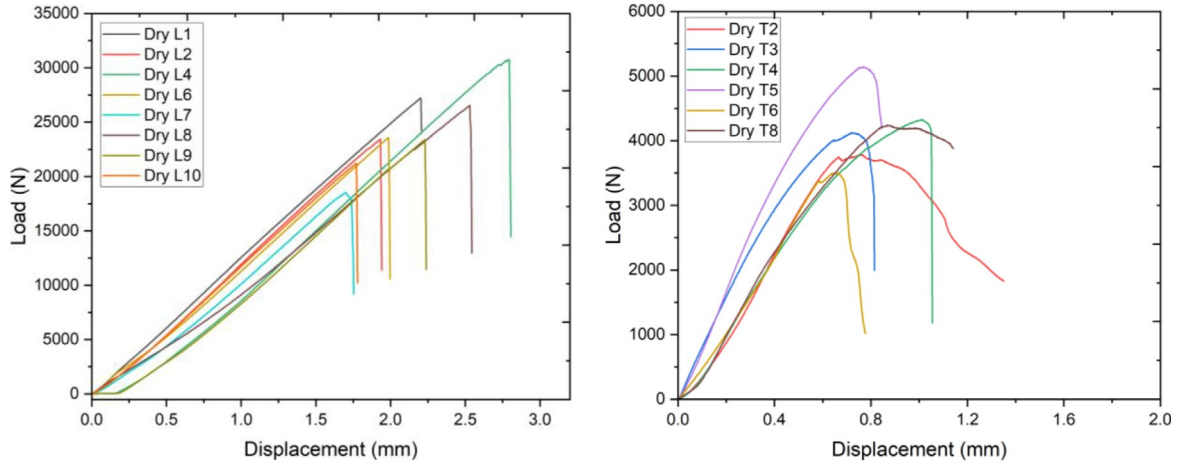

(a) Dry samples

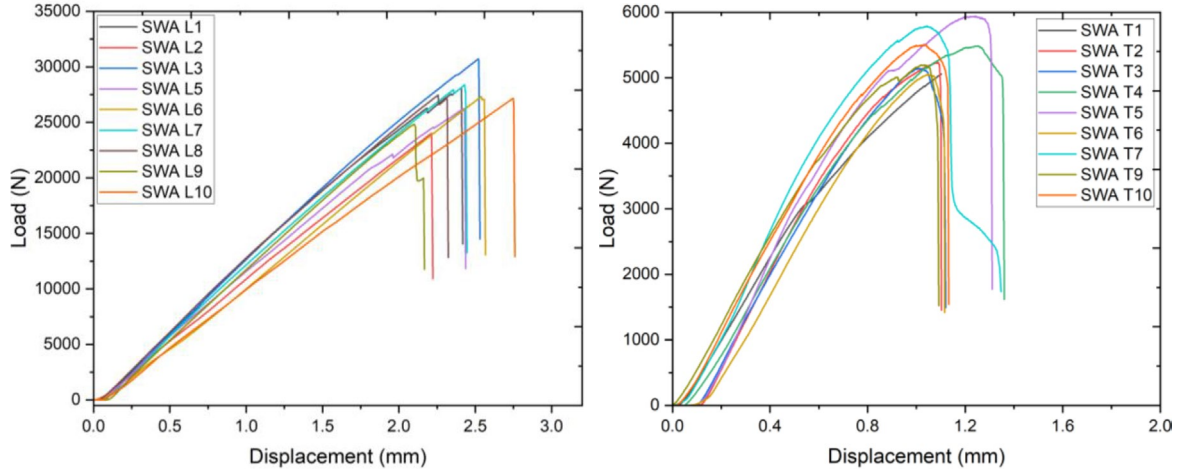

(b) SWA samples

FIGURE 10 | Load–displacement curves of [0°] and [90°] dry and SWA GF/acrylic laminate compression specimens. (a) Dry samples and (b) SWA samples.

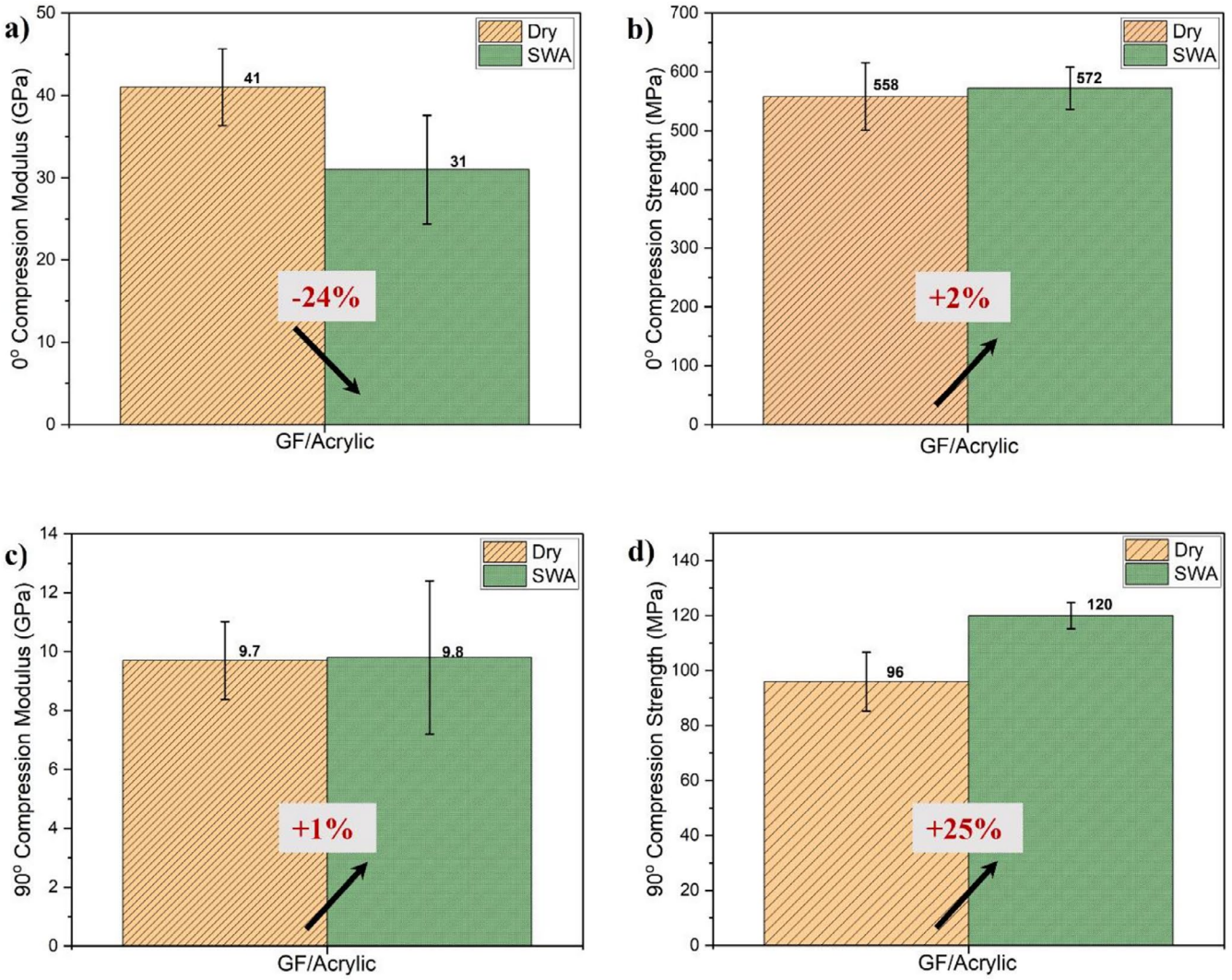

FIGURE 11 | The compressive properties of GF/acrylic composites before and after seawater ageing. The 0° compressive moduli and strengths are found in (a, b) and the 90° compressive moduli and strengths are found in (c, d).

Fibre diameter and sizing agent contribute critically towards the extent of fibre bridging and interfacial debonding in a laminate, both of which dictate its Mode I fracture toughness. Hence, this provides a valuable comparative study, as the reported composites, despite being GF/acrylic, have differences in their fibre diameter, areal weight of the reinforcement fabric and the resin grade. It is also important to note that all the reported values refer to the dry condition of the laminates. To the best knowledge of authors, there is no work reported yet on the Mode I fracture toughness of GF/acrylic composites after water ageing. The scientific insights gained from this first-ever study on Mode I fracture toughness of GF/acrylic (Elium) composites after SWA, will contribute significantly towards developing new thermoplastic composite structures for tidal and wind turbine blades and marine applications.

3.3.1 | Fractographic Study of GF/Acrylic Laminates

The fracture surfaces of the DCB tested specimen for both dry and SWA conditions are shown in Figure 8. The fibre stitching in the reinforcement and nesting of fibres during the moulding process facilitated the bridging phenomenon and caused localised fibre/matrix debonding as the crack propagated [21]. The fibre matrix debonding, fibre imprints, river markings and fibre breakages are shown in Figure 8. In SWA specimens, bare fibres and deteriorated interfacial bonding are observed (Figure 8d,e). In contrast, dry specimens exhibit intact fibre/matrix bonding, indicating a stronger interface (Figure 8b). A cohesive failure is observed in dry DCB samples (Figure 8a–c), whereas an adhesive failure is evident in the SWA samples due to interfacial debonding (Figure 8d–f).

3.4 | Compression Tests

The compression properties of GF/acrylic laminates were experimentally determined under both dry and SWA conditions. Figure 9 shows the compression test setup and the corresponding specimens before and after the compression test.

All compression tests were performed using the combined loading compression (CLC) fixture in accordance with ASTM D6641. Bending strain was continuously monitored using DIC

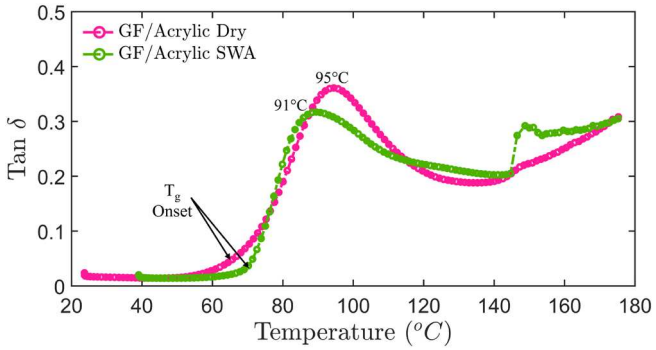

FIGURE 12 | Representative tan δ versus temperature curves for dry and SWA samples of GF/acrylic laminates.

during the tests and was found to remain within the 10% limit specified by the standard. All compression test specimens exhibited failure modes consistent with the acceptable patterns defined in ASTM D6641. The load–displacement responses for the 0° (L) and 90° (T) compression samples are shown in Figure 10a and 10b, respectively.

Figure 11 presents the compression test results for [0°] and [90°] samples under both dry and SWA conditions. A 24% reduction in compressive modulus at 0° (Figure 11a) was observed in the SWA sample compared to dry samples, which is attributed to the water ingress and interfacial debonding between the GFs and the acrylic matrix. In contrast, a notable 25% increase in compressive strength was recorded in the SWA samples with fibres in the 90° orientation (Figure 11d), which might be attributed to matrix plasticisation induced by seawater exposure. This plasticisation enhances the ductility of the acrylic matrix, contributing to improved compressive performance in the transverse direction. Additionally, a slight improvement was observed in the 0° compressive strength and the 90° compressive modulus after SWA, as shown in Figure 11b and 11c, respectively, which may be attributed to residual stress relaxation or post-conditioning stiffening effects.

Further, statistical *t*-test analysis was performed on the compression results. The variations in both 0° compressive Young's modulus and 90° compressive strength values between SWA and dry samples were statistically significant, with $p = 0.033$ and $p = 0.0035$, respectively, at a significance level of $\alpha = 0.05$. Conversely, the differences in 0° compressive strength and 90° Young's modulus between dry and SWA samples were not statistically significant, with $p = 0.068$ and $p = 0.039$, respectively.

3.5 | Dynamic Mechanical Analysis

The representative damping parameter (tan δ) versus temperature curves for dry and SWA samples are shown in Figure 12. Additionally, individual tan δ curves for each sample are provided in Figure S7.

The drops in both T_g onset and the T_g, defined as peak of the tan δ, are caused by matrix plasticisation and water ingress [4, 9, 12], which leads to a reduction in matrix moduli and strengths. Also, we wanted to observe the recovery of the T_g after allowing the sample to dry in ambient condition for 24 h. One of the SWA samples was exposed, therefore, to open air drying before DMA. All the measured T_g, values are shown in Table 3. The recovery after 24-h open-air drying indicated that the deterioration due to SWA was reversible to a large extent. The results indicate that acrylic resin exhibits a higher property retention ability upon drying of water, with significantly lower property losses after SWA compared to those observed in commonly used epoxy matrix composites [12].

TABLE 3 | Dynamic mechanical analysis results of GF/acrylic laminates.

Dynamic mechanical analysis		
Sample no	**T_g (Dry)**	**T_g (SWA)**
1	94	91
2	95	89
3	97	94[a]
Mean	95	91
SD	2	3

[a]SWA sample kept open to air at room temperature for 24 h.

Additionally, the storage modulus (G') and loss modulus (G'') as a function of temperature were shown in Figure S8a and S8b, respectively, to demonstrate the effect of SWA on the thermo-mechanical properties of the laminates. A noticeable reduction in G' and a shift in G'' peak were observed after SWA, indicating plasticisation and fibre–matrix interfacial degradation.

4 | Conclusions

In this study, the effect of SWA on Mode I fracture toughness and compressive properties of GF/acrylic matrix composites are investigated. SWA resulted in a reduction in the Mode I fracture toughness due to fibre/matrix interfacial debonding. The fracture toughness at crack initiation G_{ICI} decreased by 25% from $519.6 \pm 50.6\,J/m^2$ (dry) to $388 \pm 43\,J/m^2$ (SWA). During crack propagation G_{ICP}, a 14% reduction was observed, with values decreasing from $918.8 \pm 90.5\,J/m^2$ (dry) to $792.6 \pm 27\,J/m^2$ (SWA). Also, the *t*-test analysis revealed that the reduction in crack initiation and propagation values in SWA samples was statistically significant. These findings highlight the impact of SWA on the fracture toughness behaviour of GF/acrylic laminates. Fractographic analysis revealed that in SWA DCB specimens, a weak fibre/matrix interface led to an adhesive failure, whereas in dry DCB specimens, a strong fibre/matrix interface resulted in cohesive failure. Interestingly, the drop in Mode I fracture toughness of GF/acrylic laminates under dry and SWA condition is found to be lower than the drops reported in the literature for GF/epoxy laminates.

SWA significantly affects the compressive properties of GF/acrylic composites due to matrix plasticisation and fibre/matrix interface degradation. A 24% reduction in 0° compressive modulus is observed due to water ingress and interfacial weakening, with a marginal 2% increase in strength. In contrast, 90°

compressive strength increased by 25% under SWA, while the modulus showed a slight 1% improvement, both attributed to matrix plasticisation enhancing ductility and energy absorption ability of the composites, thereby improving transverse compressive strength. Statistical *t*-test analysis confirmed that the reduction in 0° compressive modulus and the increase in 90° compressive strength in SWA samples compared to dry samples were statistically significant, while variations in the other compressive properties were not. Additionally, a 3°C decrease in T_g was observed in SWA samples due to matrix plasticisation and interfacial debonding. A recovery in T_g was observed when the sample was air dried before subjected to DMA. This indicates that acrylic resin-based composites demonstrate good retention of properties on SWA.

This work is significant as it addresses a critical knowledge gap in the durability assessment of infusible thermoplastic composites exposed to marine environments. Unlike most seawater immersion studies that concentrate on tensile, flexural or interlaminar shear properties, this study uniquely focuses on fracture toughness and compression behaviour, which are directly linked to damage tolerance and structural stability. Understanding how seawater exposure influences crack initiation/propagation and compressive load-bearing capacity in acrylic matrix is new scientific knowledge and essential for reliable design of large structures produced with infusible thermoplastic composites. The scientific results provide application-relevant insights for the use of infusible thermoplastic composites in offshore, naval and coastal structures than conventional mechanical property evaluations alone. In particular, these insights support the optimisation, design and fatigue life assessment of GF/acrylic thermoplastic composites used in tidal and offshore wind turbine blades operating under prolonged seawater exposure.

Author Contributions

Nagappa Siddgonde: conceptualization, methodology, investigation, validation, data curation, formal analysis, visualization, writing – original draft, writing – review and editing, software. **James A. Quinn:** investigation, data curation, validation, formal analysis, visualization, writing – review and editing, conceptualization, methodology. **Conchúr M. Ó Brádaigh:** supervision, funding acquisition, validation, project administration, resources, writing – review and editing. **Dipa Ray:** conceptualization, funding acquisition, methodology, project administration, resources, validation, supervision, writing – review and editing, visualization.

Acknowledgments

The authors gratefully acknowledge Arkema GRL, France, for providing the acrylic resin used in this research. We also extend our gratitude to Johns Manville and Saertex for supplying the tailored glass fibre reinforcement.

Conflicts of Interest

The authors declare no conflicts of interest.

Data Availability Statement

The data that support the findings of this study are available from the corresponding author upon reasonable request.

References

1. LM Wind Power, "ZEBRA Project Launched to Develop First 100% Recyclable Wind Turbine Blades," accessed March 23, 2025, https://www.lmwindpower.com/en/stories-and-press/stories/news-from-lmplaces/zebra-project-launched.

2. Y. Denis, S. Nihad, G. Raphael, L. B. Philippe, D. F. Antoine, and L. Damien, "*Thermo-Chemical Modeling and Simulation of Glass/Elium Acrylic Thermoplastic Resin Composites*," Materials Research Proceedings (Materials Research Forum LLC, 2023): 313–320, https://doi.org/10.21741/9781644902479-34.

3. A. Hassan, R. Khan, N. Khan, M. Aamir, D. Y. Pimenov, and K. Giasin, "Effect of Seawater Ageing on Fracture Toughness of Stitched Glass Fibre/Epoxy Laminates for Marine Applications," *Journal of Marine Science and Engineering* 9 (2021): 196, https://doi.org/10.3390/jmse9020196.

4. C. Floreani, "Interlaminar Fracture Behaviour of Fibre Reinforced Powder Epoxy Composites" (PhD thesis, School of Engineering, The University of Edinburgh, 2022).

5. J. A. Rodríguez-González and C. Rubio-González, "Seawater Effects on Interlaminar Fracture Toughness of Glass Fibre/Epoxy Laminates Modified With Multiwall Carbon Nanotubes," *Journal of Composite Materials* 55 (2021): 387–400, https://doi.org/10.1177/0021998320950788.

6. M. Devine, A. Bajpai, W. Obande, C. M. Ó Brádaigh, and D. Ray, "Seawater Ageing of Thermoplastic Acrylic Hybrid Matrix Composites for Marine Applications," *Composites Part B, Engineering* 263 (2023): 110879, https://doi.org/10.1016/j.compositesb.2023.110879.

7. D. Stankovic, W. Obande, M. Devine, A. Bajpai, C. M. Ó Brádaigh, and D. Ray, "Accelerated Seawater Ageing and Fatigue Performance of Glass Fibre Reinforced Thermoplastic Composites for Marine and Tidal Energy Applications," *Composites Part C: Open Access* 14 (2024): 100470, https://doi.org/10.1016/j.jcomc.2024.100470.

8. W. Obande, C. M. Ó Brádaigh, and D. Ray, "Continuous Fibre-Reinforced Thermoplastic Acrylic-Matrix Composites Prepared by Liquid Resin Infusion – A Review," *Composites Part B, Engineering* 215 (2021): 108771, https://doi.org/10.1016/j.compositesb.2021.108771.

9. H. Bel Haj Frej, R. Léger, D. Perrin, and P. Ienny, "A Novel Thermoplastic Composite for Marine Applications: Comparison of the Effects of Aging on Mechanical Properties and Diffusion Mechanisms," *Applied Composite Materials* 28 (2021): 899–922, https://doi.org/10.1007/s10443-021-09903-0.

10. L. C. M. Barbosa, M. Santos, T. L. L. Oliveira, G. F. Gomes, and A. C. Ancelotti Junior, "Effects of Moisture Absorption on Mechanical and Viscoelastic Properties in Liquid Thermoplastic Resin/Carbon Fibre Composites," *Polymer Engineering and Science* 59 (2019): 2185–2194, https://doi.org/10.1002/pen.25221.

11. N. H. Nash, A. Portela, C. I. Bachour-Sirerol, I. Manolakis, and A. J. Comer, "Effect of Environmental Conditioning on the Properties of Thermosetting- and Thermoplastic-Matrix Composite Materials by Resin Infusion for Marine Applications," *Composites Part B: Engineering* 177 (2019): 107271, https://doi.org/10.1016/j.compositesb.2019.107271.

12. P. Davies, P.-Y. Le Gac, and M. Le Gall, "Influence of Sea Water Aging on the Mechanical Behaviour of Acrylic Matrix Composites," *Applied Composite Materials* 24 (2017): 97–111, https://doi.org/10.1007/s10443-016-9516-1.

13. M. Devine, D. Hornsby, C. M. Ó Brádaigh, and D. Ray, "Sizing Agents and Their Effect on the Water Absorption Behaviour of GF/Acrylic Composites," 21st European Conference on Composite Materials, Nantes, France: ECCM21, 2004.

14. A. Couture, J. Laliberte, and C. Li, "Mode I Fracture Toughness of Aerospace Polymer Composites Exposed to Fresh and Salt Water,"

Chemical and Materials Engineering 1 (2013): 8–17, https://doi.org/10.13189/cme.2013.010102.

15. A. Bolluk, M. Devine, J. A. Quinn, and D. Ray, "Repair of Acrylic/Glass Composites by Liquid Resin Injection and Press Moulding," *Composites Part B: Engineering* 281 (2024): 111513, https://doi.org/10.1016/j.compositesb.2024.111513.

16. S. K. Bhudolia, P. Perrotey, and S. C. Joshi, "Mode I Fracture Toughness and Fractographic Investigation of Carbon Fibre Composites With Liquid Methylmethacrylate Thermoplastic Matrix," *Composites Part B: Engineering* 134 (2018): 246–253, https://doi.org/10.1016/j.compositesb.2017.09.057.

17. M. E. Kazemi, L. Shanmugam, D. Lu, X. Wang, B. Wang, and J. Yang, "Mechanical Properties and Failure Modes of Hybrid Fibre Reinforced Polymer Composites With a Novel Liquid Thermoplastic Resin, Elium," *Composites Part A: Applied Science and Manufacturing* 125 (2019): 105523, https://doi.org/10.1016/j.compositesa.2019.105523.

18. V. Kaushik and A. Ghosh, "Experimental and Numerical Characterization of Mode I Fracture in Unidirectional CFRP Laminated Composite Using XIGA-CZM Approach," *Engineering Fracture Mechanics* 211 (2019): 221–243, https://doi.org/10.1016/J.ENGFRACMECH.2019.01.038.

19. W. Obande, D. Mamalis, D. Ray, L. Yang, and C. M. Ó Brádaigh, "Mechanical and Thermomechanical Characterisation of Vacuum-Infused Thermoplastic- and Thermoset-Based Composites," *Materials & Design* 175 (2019): 107828, https://doi.org/10.1016/j.matdes.2019.107828.

20. N. Han, O. Yuksel, J. S. M. Zanjani, L. An, R. Akkerman, and I. Baran, "Experimental Investigation of the Interlaminar Failure of Glass/Elium Thermoplastic Composites Manufactured With Different Processing Temperatures," *Applied Composite Materials* 29 (2022): 1061–1082, https://doi.org/10.1007/s10443-021-10000-5.

21. X. Zhang and Z. Deng, "Effects of Seawater Environment on the Degradation of GFRP Composites by Molecular Dynamics Method," *Polymers* 14 (2022): 2804, https://doi.org/10.3390/polym14142804.

Supporting Information

Additional supporting information can be found online in the Supporting Information section. **Figure S1:** Mode-I DCB specimens for both dry and seawater aged conditions. **Figure S2:** Average water absorption curves of the four compression samples. **Figure S3:** Load versus displacement responses for both dry and SWA DCB samples. **Figure S4:** Load versus displacement response for both dry and SWA DCB samples. **Figure S5:** The critical SERR versus crack growth during Mode I fracture toughness tests for both dry and SWA conditions. **Figure S6:** The critical SERR versus crack growth during Mode I fracture toughness tests for both dry and SWA conditions. **Figure S7:** Tan(δ) versus temperature curves for dry and SWA samples of GF/acrylic laminates. The GF/Acrylic SWA3* sample were air-dried at room temperature for 24 h before testing. **Figure S8:** DMA curves; (a) storage modulus versus temperature; (b) loss modulus versus temperature. **Table S1:** All experimental results of GF/acrylic composites under dry and aged conditions.